THE JOURNAL OF PHYSICAL CHEMISTRY C
A JOURNAL OF THE AMERICAN CHEMICAL SOCIETY

pubs.acs.org/JPCC

Article

Stimulating the Pre-Catalyst Redox Reaction and the Proton–Electron Transfer Process of Cobalt Phthalocyanine for CO_2 Electroreduction

Hengyu Li, Jie Wei, Xuya Zhu, Lin Gan, Tao Cheng, and Jia Li*

Cite This: *J. Phys. Chem. C* 2022, 126, 9665–9672

Read Online

ACCESS | Metrics & More | Article Recommendations | Supporting Information

ABSTRACT: The mechanism for electrochemical carbon dioxide reduction reaction (CO_2RR) to carbon monoxide on cobalt phthalocyanine (CoPc) in aqueous electrolytes remains debatable, impeding the design of high-performance catalysts. By using a quasi-empirical protocol with density functional theory calculations, we identify the mechanisms of two important steps for CO_2RR on CoPc: the reduction of $Co^{II}Pc$ to form catalytically active $[Co^{II}Pc]^{2-}$ for CO_2 adsorption and the proton–electron transfer to the key intermediate $[CoPc\text{-}COO]^{2-}$ to form $[CoPc\text{-}COOH]^{2-}$. According to the charge states and pK_a analysis, the formation of the adsorbed carboxyl (*COOH) takes place via the concerted proton–electron transfer process at low potentials, and the sequential proton–electron transfer process becomes thermodynamically favored at more reductive potentials, which successfully elucidates the potential-dependent reaction kinetics of CO_2RR on CoPc catalysts. Electron-withdrawing substituents of CoPc would enhance the reduction of CoPc but hinder the protonation of $*CO_2$, which accounts for previous conflicting results. Our findings not only deepen the understanding of CoPc-catalyzed CO_2RR but also provide a guideline for molecular engineering of CoPc-based catalysts.

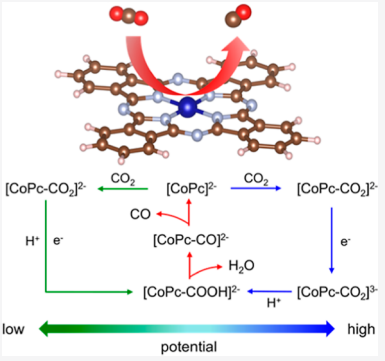

INTRODUCTION

Excessive exploitation and utilization of conventional fossil fuels have led to a high concentration of atmospheric CO_2, causing severe environmental and climatic problems.[1,2] Electrocatalytic CO_2 reduction reaction (CO_2RR), because of its mild condition and controllable production, is considered an ideal approach to converting CO_2 into useful chemicals and reaching the goal of a carbon-neutral economy.[3,4] For CO_2 reduction to CO, metallo-phthalocyanines have emerged as promising electrocatalysts in recent years due to their maximum atom efficiency, low overpotential, and high selectivity.[5−7] In particular, cobalt phthalocyanine (CoPc) has been demonstrated to be the most active for CO_2 reduction to CO.[8−14] Near Faradaic unity efficiencies to CO and onset overpotentials as low as 170 mV have also been reported.[9,13,14]

However, the reaction mechanism of CO_2RR on CoPc is still a topic of debate. It is generally believed that CO_2RR on CoPc begins after the reduction of $Co^{II}Pc$ to $[Co^{I}Pc]^{-}$, and Co^{I} is the active site.[8,15−17] However, this is contradictory to recent in situ X-ray absorption spectroscopy results, which suggests that the oxidation state of cobalt remains +2 throughout the reaction process.[18,19] The inconsistency originates from an insufficient understanding of the redox properties and electronic configurations of reaction intermediates. Besides, whether the reaction steps follow a concerted proton–electron transfer (CPET) process or a sequential PET (SPET) process is also under discussion.[20] Experimental kinetic studies show that the reaction shifts from CPET-dominant to SPET-dominant as the applied potential becomes more reductive.[21] However, none of the theoretical studies provide insights into the potential-dependent kinetics of the electron transfer process.

The incomprehensive reaction mechanism has limited the rational modification of CoPc to achieve better performance. Both electron-donating[12,17] and electron-withdrawing[22,23] substituents have been investigated and reported to improve the catalytic performance of CoPc. For instance, perfluorinated cobalt phthalocyanine ($CoPcF_{16}$) was reported to have better activity,[24] while a later study showed even lower activity of $CoPcF_{16}$ compared to the pristine CoPc.[25] The conflicting phenomena result in difficulty in providing the strategy for the modification of CoPc.

Herein, we perform density functional theoretical (DFT) calculations of the electroreduction mechanism of CO_2 to CO on CoPc by considering previously overlooked charge states and electronic configurations of reaction intermediates at the working potentials. Based on the charge states of intermediates, we reveal a full picture of the potential-dependent

Received: February 15, 2022
Revised: May 19, 2022
Published: June 3, 2022

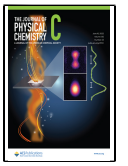

https://doi.org/10.1021/acs.jpcc.2c01125
J. Phys. Chem. C 2022, 126, 9665−9672

concerted and non-concerted (sequential) PET processes of the CO_2 reduction mechanism on CoPc, which successfully accounts for the experimentally observed potential dependence of reaction kinetics. Based on this, we further evaluate the influence of different substituents on the CO_2RR activity of CoPc, which helps understand the contradictory positive effects of electron-donating or electron-withdrawing groups substituted in CoPc. Our results provide important guidelines for the design of new CoPc-based CO_2RR electrocatalysts.

METHODS

All spin-polarized DFT calculations were performed using the Vienna ab initio simulation package (VASP).[26,27] Electronic structures and redox potentials of CoPc intermediates were calculated with the revised Heyd−Scuseria−Ernzerhof-screened hybrid functional (HSE06),[28] while the rest of the calculations were carried out with the DFT + U method[29,30] on account of the computational cost. An effective U of 4 eV was used because it can provide an accurate energy level of d states for the Co of CoPc compared to the valence-band photoelectron spectra,[31] and the adsorption energies of key intermediates calculated are in agreement with the HSE06 results (Section S1 in the Supporting Information). In all calculations, the energy cutoff of the plane wave basis set was 500 eV. Only Gamma points were used for the Brillouin zone sampling. All atoms were relaxed until the force on each atom was less than 0.01 eV/Å. The D3 functional was employed to describe the nonnegligible van der Waals interactions.[32,33]

A continuum dielectric model as implemented in the VASPsol code[34,35] was used to simulate the aqueous environment. To obtain more accurate redox potentials and pK_a values as well as to investigate the effect of hydrogen bonding, we employed a micro-solvation model with two explicit water molecules for intermediates with carboxyl groups.[36,37] However, we did not add any explicit water molecules to the geometry of $[CoPc\text{-}CO]^{n-}$ because ab initio molecular dynamics simulations showed that the adsorbed carbon monoxide could hardly form hydrogen bonds with water. (Section S2 in the Supporting Information).

The one-electron redox potential of the $A^{(n+1)-}/A^{n-}$ couple relative to the reversible hydrogen electrode (RHE) was calculated as

$$U^{o}_{RHE} = -\frac{\Delta G^{o}}{F} - U^{toSHE} + 0.0592 \times pH$$

where F is the Faradayconstant; ΔG^{o} is the Gibbs free energy difference between $A^{(n+1)-}$ and A^{n-}; and U^{toSHE} is the reference potential for the standard hydrogen electrode (SHE), and the value of 4.6 V[38] was employed. The pH was set to 7 to be comparable to the experimental data. However, the as-calculated absolute redox potentials using the hybrid DFT or DFT + U method would have systematic errors, which have been reported in the literature,[39,40] although these methods are believed to provide accurate predictions of electronic configurations. The errors and corresponding corrections will be discussed in the following section based on the calculated data.

The free energy profiles involve the following molecule adsorption/desorption steps

$$[CoPc]^{n-} + CO_2 \rightarrow [CoPc\text{-}CO_2]^{n-} \quad (a)$$

$$[CoPc\text{-}CO]^{n-} \rightarrow [CoPc]^{n-} + CO \quad (b)$$

electron transfer (ET) steps

$$[CoPc\text{-}CO_2]^{n-} + e^- \rightarrow [CoPc\text{-}CO_2]^{(n+1)-} \quad (c)$$

$$[CoPc]^{n-} + e^- \rightarrow [CoPc]^{(n+1)-} \quad (d)$$

proton transfer (PT) steps

$$[CoPc\text{-}CO_2]^{(n+1)-} + H^+ \rightarrow [CoPc\text{-}COOH]^{n-} \quad (e)$$

$$[CoPc\text{-}COOH]^{(n+1)-} + H^+ \rightarrow [CoPc\text{-}CO]^{n-} + H_2O \quad (f)$$

and CPET steps

$$[CoPc\text{-}CO_2]^{n-} + H^+ + e^- \rightarrow [CoPc\text{-}COOH]^{n-} \quad (g)$$

$$[CoPc\text{-}COOH]^{n-} + H^+ + e^- \rightarrow [CoPc\text{-}CO]^{n-} + H_2O \quad (h)$$

To calculate the free energy change of these steps, we considered the free energy with the gas phase correction.[41] For ET steps, the free energy changes of step (c) (ΔG_c) and step (d) (ΔG_d) were calculated with corrected redox potentials

$$\Delta G_c = -e(U^{o,cor}_{RHE}([CoPc\text{-}CO_2]^{n-}/[CoPc\text{-}CO_2]^{(n+1)-}) - U)$$

$$\Delta G_d = -e(U^{o,cor}_{RHE}([CoPc]^{n-}/[CoPc]^{(n+1)-}) - U)$$

where U is the applied potential on the RHE scale. For the PT step (e), the pK_a of $[CoPc\text{-}COOH]^{n-}$ was calculated using the isodesmic proton−exchange reaction scheme[37] to determine whether the protonation is spontaneous at the operative pH (Section S3 in Supporting Information). Then, the free energy change of step (e) (ΔG_e) was calculated as

$$\Delta G_e = -2.303\ RT^{*}pK_a + 0.0592\ pH$$

For the CPET step (g), the free energy change (ΔG_g) was calculated directly by adding the items of ΔG_c and ΔG_e

$$\Delta G_g = \Delta G_c + \Delta G_e$$

The well-established computational hydrogen electrode (CHE) model[42] was not used, with which the free energy change of a CPET step (ΔG_{CHE}) was calculated as

$$A + H^+ + e^- \rightarrow AH$$

$$\Delta G_{CHE} = G(AH) - G(A) - \frac{1}{2}G(H_2)$$

Because

$$G(AH) - G(A) = [G(AH) - G(A^-)] + [G(A^-) - G(A)]$$

$$= PA + EA + G(H^+) + G(e^-)$$

where PA is the proton affinity of A^- and EA is the electron affinity of A; the systematic errors in calculating PA and EA would also lead to an error in ΔG_{CHE}. In our case, we found that the free energy change of the potential-deciding step calculated with the CHE model strongly disagrees with the experimental value (Supporting Information Section S1), so the CHE model was considered to be inadequate for the quantitative study of reaction mechanisms. Finally, the free energy changes of steps (f) and (h) were not directly

https://doi.org/10.1021/acs.jpcc.2c01125
J. Phys. Chem. C 2022, 126, 9665−9672

calculated but were derived by the free energy change of the overall reaction minus the other steps.

Since previous experimental studies suggested that the reaction rate is pH-dependent,[8,21,24] the free energies of the transition states of the proton-involved steps were calculated to ascertain the rate-determining steps (RDS). The climbing image nudged elastic band (CI-NEB)[43,44] method was used to locate the transition states. Bicarbonate was used as the proton source because the pK_a of bicarbonate (10.3) was smaller than the pK_a of H_2O (14.0).[45] The PT steps have the initial and final states with the same number of electrons so that the direct CI-NEB calculation would be adequate. However, a CPET step has the initial and final states with a different number of electrons. To determine the transition state of CPET steps, we employed the grand canonical potential kinetics (GCP-K) method[46] and assumed that the electron numbers of intermediates could only be integers for molecular catalysts. (Section S4 in the Supporting Information).

RESULTS & DISCUSSION

Redox Properties and Valence States of $[CoPc]^{n-}$. As shown in Figure 1, the calculated structure of CoPc has a D_{4h} symmetry, and the Co−N bond length is 1.917 Å, which is in good agreement with the experimental value of 1.91 Å.[47] Figure S5 shows the projected density of states (PDOSs) for CoPc. The Co atom in the CoPc has seven 3d electrons, and the electronic configuration is $d^2_{xy}d^2_{xz}d^2_{yz}d^1_{z2}$. Valence-band photoelectron spectroscopy (PES) measurements showed that the highest occupied molecular orbital (HOMO) peak contains purely ligand states,[48,49] which agrees with the nonmetallic HOMO predicted by the calculation. The ligand also contributes to most of the lowest unoccupied molecular orbital (LUMO) peaks. Only low-intensity d_π states are found to be present in the LUMO. These states originate in a hybridization of the metal d orbitals with the aza-bridge nitrogen p_z orbitals, which are directed on the diagonal axes of the molecule and out of the molecular plane.[31] The calculated ground state of $[CoPc]^-$ is $[Co^{II}Pc]^-$ with the electronic configuration of $d^2_{xy}d^2_{xz}d^1_{yz}d^2_{z2}$ for Co 3d electrons, and the phthalocyanine ligand is solely reduced. The unpaired electrons on the Co atom and those on the ligand are in opposite spin states. With the reduction of the ligand, the symmetry of the CoPc molecule decreases to D_{2h}. Moreover, the Co−N bond lengths along the two axes are 1.918 and 1.903 Å, respectively. The reduction on the Co with the electronic configuration of $d^2_{xy}d^2_{xz}d^2_{yz}d^2_{z2}$ is found to be 0.22 eV higher than the ground state in which the ligand is reduced. The second reduction of CoPc also occurs on the ligand, with Co remaining in the +2 oxidation state. The statement of unreduced Co metal is inconsistent with the previous opinion but is reasonable since the ligand contributes to the LUMO of CoPc.

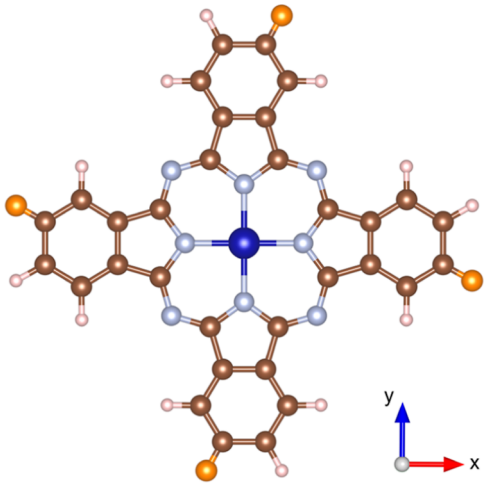

Figure 1. Molecular structure of a typical CoPc-based catalyst ($CoPcX_4$). Brown, pink, gray, and blue spheres represent C, H, N, and Co atoms, respectively. The orange spheres represent an arbitrary functional group X (X = H atom for pristine CoPc).

Redox Potentials and Reaction Mechanisms. In comparing the theoretical and experimental results, we performed electrochemical characterization of the redox potentials for CoPc in CO_2-saturated aqueous solution of 0.1 M $KHCO_3$ (pH = 6.71), which is a common operative condition for CO_2RR. In the cyclic voltammogram of CoPc (Figure S6a), two pairs of redox peaks with the reduction waves at around −0.07 and −0.33 V (vs RHE) are observed, which represent the reduction reaction of CoPc/$[CoPc]^-$ and $[CoPc]^-/[CoPc]^{2-}$, respectively.[50,51] Compared with the experimental results, the calculated absolute reduction potentials, as listed in Table1, are much more negative.

Table 1. Calculated Absolute (abs.) and Corrected (cor.) Redox Potentials of Reaction Intermediates. * Experimental Value was used for the $[CoPc]^-/[CoPc]^{2-}$ and $[CoPc]^-/[CoPc]^{2-}$ Redox Couple

reduced	oxidized	redox potential (abs., vs RHE)	redox potential (cor.)
$[CoPc]^-$	[CoPc]	−0.746 V	−0.07 V*
$[CoPc]^{2-}$	$[CoPc]^-$	−1.096 V	−0.33 V*
$[CoPc\text{-}CO_2]^{2-}$	$[CoPc\text{-}CO_2]^-$	−0.702 V	0.019 V
$[CoPc\text{-}CO_2]^{3-}$	$[CoPc\text{-}CO_2]^{2-}$	−1.115 V	−0.394 V
$[CoPc\text{-}COOH]^-$	[CoPc-COOH]	−0.722 V	−0.001 V
$[CoPc\text{-}COOH]^{2-}$	$[CoPc\text{-}COOH]^-$	−0.944 V	−0.223 V
$[CoPc\text{-}COOH]^{3-}$	$[CoPc\text{-}COOH]^{2-}$	−1.665 V	−0.944 V
$[CoPc\text{-}CO]^-$	[CoPc-CO]	−0.832 V	−0.111 V
$[CoPc\text{-}CO]^{2-}$	$[CoPc\text{-}CO]^-$	−1.006 V	−0.285 V
$[CoPc\text{-}CO]^{3-}$	$[CoPc\text{-}CO]^{2-}$	−1.743 V	−1.022 V

However, their potential difference (0.35 V) is basically consistent with the experimental result (0.26 V). Following previous suggestions that the relative hybrid DFT redox potentials are more reliable than the absolute values,[52] we used the experimentally measured redox potential values of CoPc/$[CoPc]^-$ and $[CoPc]^-/[CoPc]^{2-}$ as references to calibrate the calculated absolute redox potentials of the following key intermediate species (namely, corrected redox potentials), such as $[CoPc\text{-}CO_2]^{2-}$, $[CoPc\text{-}COOH]^{2-}$, [CoPc-CO], and so forth, as listed in Table 1.

The average reported onset potential of CO_2RR to CO on CoPc is −0.34 V versus RHE.[14,23,53,54] At this potential, according to the experimental redox potential, CoPc is reduced to $[CoPc]^{2-}$. In addition, CoPc-CO_2, CoPc-COOH, and CoPc-CO are all predicted to be in the charge state of −2 at the onset potential according to the calculated redox potentials. The charge states of intermediates indicate that the formation of *COOH and *CO follows the CPET

https://doi.org/10.1021/acs.jpcc.2c01125
J. Phys. Chem. C 2022, 126, 9665−9672

pathway, as indicated by the red and green arrows in Figure 2a, and the energy profile of the whole reaction is shown in Figure

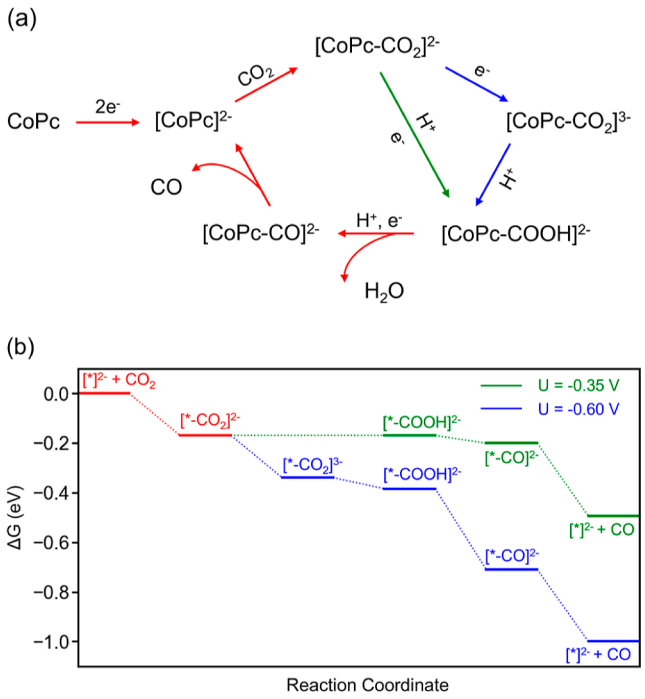

Figure 2. (a) Schematic mechanism and (b) free energy profile of CO_2 reduction at different applied potentials, where * represents the CoPc molecule.

2b. The possibility of the SPET pathway for the formation of *COOH and *CO was also considered. In the PT step for the formation of *COOH, the charge states of CoPc-CO_2 and CoPc-COOH are −2 and −1, respectively. However, the pK_a of $[CoPc\text{-}COOH]^-$ is 3.5, indicating the minimal protonation of $[CoPc\text{-}CO_2]^{2-}$ at an operative pH. Meanwhile, since the intermediate CoPc-COOH is in the charge state of −2, the PT step in the SPET pathway for the formation of *CO is

$$[CoPc\text{-}COOH]^{2-} + H^+ \rightarrow [CoPc\text{-}CO]^- + H_2O$$

which is thermodynamically endothermic with ΔG = +0.04 eV.

Therefore, the formation of *COOH and *CO can hardly occur according to the SPET pathway. In addition, with the above-mentioned CPET pathways, the onset potential of CO_2RR to CO on CoPc is calculated to be −0.35 V versus RHE, which agrees well with the experimental values of −0.34 V, validating our method to calculate the free energy differences of CPET pathways precisely. At more negative potentials (U = −0.60 V vs RHE was taken as an example here), $[CoPc\text{-}CO_2]^{2-}$ can be reduced to $[CoPc\text{-}CO_2]^{3-}$, while the charge states of other intermediates remain unchanged. Thus, the formation of *COOH follows the SPET pathway. The overall reaction pathway is indicated by the red and blue arrows in Figure 2a, and the energy profile is shown in Figure 2b. In addition, the calculated pK_a of $[CoPc\text{-}COOH]^{2-}$ is 7.73, so the protonation of $[CoPc\text{-}CO_2]^{3-}$ spontaneously occurs at operative pH in thermodynamics, which further supports the SPET pathway.

In kinetics, at the low overpotential (U_1 = −0.35 V), the formation of *COOH has a higher energy barrier of 0.89 eV (Table 2), which is the RDS of the reaction. However, the protonation of $[CoPc\text{-}CO_2]^{3-}$ is the RDS with a higher energy

Table 2. Energy Barriers of the Proton-Involved Reaction Steps at U_1 = −0.35 V and U_2 = −0.60 V

reaction step	ΔG_{TS} (eV, U_1)	ΔG_{TS} (eV, U_2)
$[*\text{−}CO_2]^{2-} + H^+ + e^- \rightarrow [*\text{−}COOH]^{2-}$	0.89	/
$[*\text{−}CO_2]^{3-} + H^+ \rightarrow [*\text{−}COOH]^{2-}$	/	0.67
$[*\text{−}COOH]^{2-} + H^+ + e^- \rightarrow [*\text{−}CO]^{2-} + H_2O$	0.26	0.15

barrier of 0.67 eV (Table 2) at a high overpotential (U_2 = −0.60 V). Thus, the potential-dependent kinetics of CO_2 reduction on CoPc[21] can be well explained by the above results. At low overpotentials where CoPc-CO_2 can hardly be reduced to $[CoPc\text{-}CO_2]^{3-}$, the RDS (formation of *COOH) takes place through the CPET pathway. As the applied potential shifts more negative, more intermediates are in the charge state of −3, and the reaction can shift from CPET-dominant to SPET-dominant. Thus, the charge state of CoPc-CO_2 is the key factor in the potential-dependent kinetics of CO_2 reduction. However, the reaction mechanism at highly reductive potentials (<−1 V vs RHE) where the intermediates are in higher charge states will not be discussed here, as mass transport becomes an important factor in the reaction kinetics in this potential range.[18]

It is noted that the adsorption of CO_2 is the first step for the reaction. As shown in Figure 3a, CO_2 is only physisorbed on neutral CoPc, while it can adopt a bent geometry and become chemisorbed on $[CoPc\text{-}CO_2]^{2-}$, as shown in Figure 3b. Hydrogen bonding also plays an essential part in the adsorption of CO_2. The length of the Co−C bond in $[CoPc\text{-}CO_2]^{2-}$ is 2.13 Å when the structure is optimized in a fully implicit solvent. With the addition of explicit water molecules, the bond length is shortened to 2.01 Å, as shown in Figure 3c. The PDOS of Co in CoPc and C in CO_2 indicates that the σ bond of Co−C is a hybridization of Co-d_{z^2} and C-p_z, as shown in Figure 3d. Hydrogen bonding can exert a drawing effect on the electrons of $[CoPc\text{-}CO_2]^{2-}$. The increased intensity of C-p_z indicates that more electrons are drawn into the bonding state, and thus the adsorption of CO_2 is enhanced.

Modification of CoPc. Based on our proposed mechanism, we discuss how the substituents would influence the CO_2RR activity of CoPc in the following. The derivatives that we investigated are in the form of $CoPcX_4$ (Figure 1). The Hammett constant (σ_p) was used to evaluate the charge effect induced by the substituents, which was defined by Hammett from the ionization constant of benzoic acid (K_H) and the ionization constant of a para-substituted benzoic acid (K_X) in the water at 25 °C

$$\sigma_p = \lg K_X - \lg K_H.$$

Previous studies which assumed the Co center to be the redox site showed that the electron-withdrawing groups could facilitate the reduction of the Co center, and the correlation between redox potentials and the Hammett constant of substituents is approximately linear.[54] Interestingly, as shown in Figure 4a, our results are in good agreement with the experimental trends, although the reductions occur on the ligand in our calculation. In actual reactions, due to the aggregation of molecules, the CoPc may need more reductive potential to be reduced than predicted in theory.[55] In addition, it has been reported that only a fraction of CoPc sites can be reduced to being electrochemically active at the working potential.[53,54] Since the chemisorption of CO_2 requires the

https://doi.org/10.1021/acs.jpcc.2c01125
J. Phys. Chem. C 2022, 126, 9665−9672

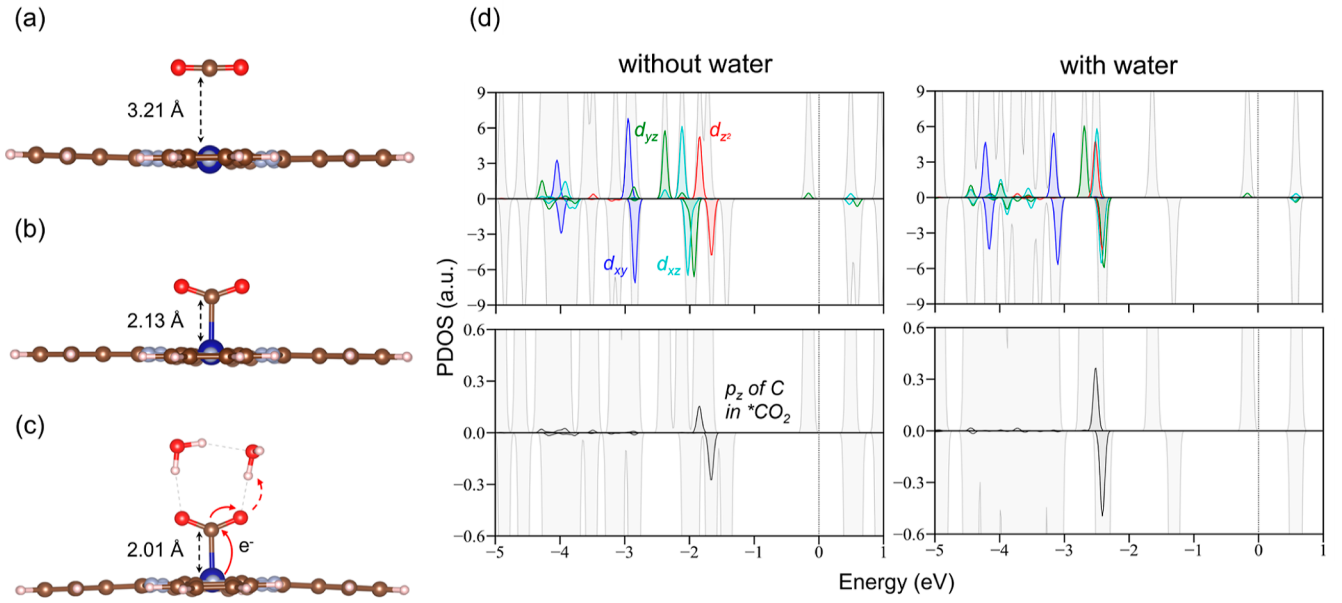

Figure 3. Atomic structures of (a) CoPc-CO_2, (b) $[CoPc\text{-}CO_2]^{2-}$, and (c) $[CoPc\text{-}CO_2]^{2-}$ with two explicit water molecules. (d) Projected density of states of Co and C in CO_2 for $[CoPc\text{-}CO_2]^{2-}$ with and without explicit water molecules. The energy level of HOMO is set to be 0 eV. The total density of states is represented in gray, d_{z^2} in red, d_{xz} in cyan, d_{yz} in green, d_{xy} in blue, and p_z in black, respectively.

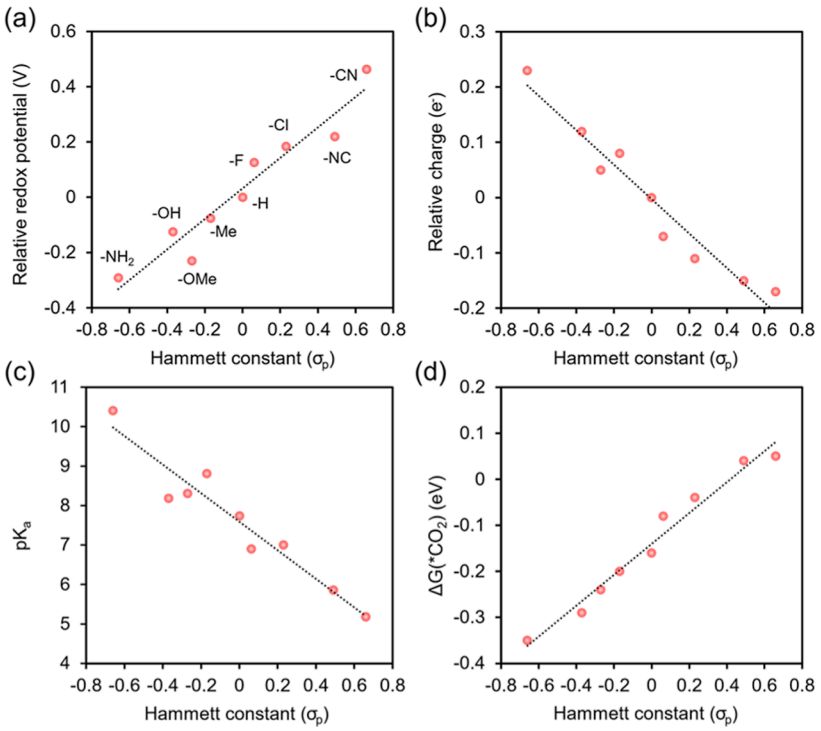

Figure 4. Correlations between the para position Hammett constant (σ_{para}) of substituent X and (a) redox potential of $[CoPcX_4]^{-}/[CoPcX_4]^{2-}$ relative to $[CoPc]^{-}/[CoPc]^{2-}$, (b) charge of the central part of $[CoPcX_4\text{-}CO_2]^{2-}$ relative to $[CoPc\text{-}CO_2]^{2-}$, (c) pK_a of $[CoPcX_4\text{-}COOH]^{2-}$, and (d) adsorption free energy of CO_2 on $[CoPcX_4]^{2-}$. The Hammett constants are taken from experimental data.[57]

CoPc to be in the charge state of −2, the enhanced reduction can increase the number of active sites and promote the observed activity with the electron-withdrawing groups.

However, the electron-withdrawing substituents also lead to decreased charge density around the central active part (Figure 4b, the central active part refers to the atoms except those in the outer benzene rings), which would weaken the Coulomb interaction between the adsorbed CO_2 and hydrogen, resulting in a lower pK_a of $[CoPcX_4\text{-}COOH]^{2-}$ (Figure 4c) and thus hindering the kinetics of PT. Meanwhile, because the adsorbed CO_2 adopts a bent structure, the adsorption is stabilized by the interaction between the dipole of *CO_2 and the local electric field.[56] The weaker dipole-filed interaction caused by the lower charge density around the active center would lead to the weaker adsorption of CO_2 (Figure 4d) and hinder the occurrence of the reaction, which is consistent with the observation of in situ scanning tunneling microscopy.[25] The optimal modification strategy for the improved activity of

https://doi.org/10.1021/acs.jpcc.2c01125
J. Phys. Chem. C 2022, 126, 9665−9672

CoPc should be proposed in consideration of the redox potential, pK_a, and CO_2 adsorption. If the molecules can be well dispersed and the ET problem can be overcome so that there is no need to enhance the reduction of CoPc to increase the number of active sites, the electron-donating substituents could show their advantage in boosting the adsorption of CO_2 and promoting the reaction kinetics, while if the reduction of CoPc remains to be the major constraint on the CO_2RR kinetics, the activity can be improved with electron-withdrawing substituents.

CONCLUSIONS

In summary, our study revealed the reaction mechanism of electrochemical CO_2 reduction to CO on CoPc through DFT calculations. The $Co^{II}Pc$ molecule is first electrochemically reduced to a charged $[Co^{II}Pc]^{2-}$ with the valence state of the Co center remaining unchanged, which, with the aid of water, is a necessary process for the adsorption of CO_2. The reaction pathway and kinetics are determined by the charge states of intermediates. At the onset potential, the RDS is the formation of *COOH, which follows a CPET pathway. At more reductive potentials, the SPET pathway becomes thermodynamically favored, which leads to the potential-dependent reaction kinetics. The inductive effect of substituents is essential to the activity of CoPc-based catalysts. The electron-withdrawing substituents can facilitate the reduction of CoPc to the charged $[Co^{II}Pc]^{2-}$ but are disadvantageous in the adsorption of CO_2 and PT, thereby playing dual roles of the coin. For CoPc molecules well dispersed on the conductive support, which also facilitates a facile electroreduction of CoPc, an electron-donating substitute would be a better choice to facilitate the key PT to the $[Co^{II}Pc\text{-}COO]^{2-}$ intermediate. Our results are helpful in rationally designing efficient catalysts for electrochemical CO_2 reduction.

ASSOCIATED CONTENT

Supporting Information

The Supporting Information is available free of charge at https://pubs.acs.org/doi/10.1021/acs.jpcc.2c01125.

Comparison of binding energies calculated by HSE06 and PBE + *U*, micro-solvation structures of intermediates, isodesmic proton−exchange reaction scheme, GCP-K, atomic structures of transition states, relative energies for intermediates in different spin states, and electrochemical characterization of redox potentials (PDF)

AUTHOR INFORMATION

Corresponding Author

Jia Li − *Institute of Materials Research and Shenzhen Geim Graphene Center, Shenzhen International Graduate School, Tsinghua University, Shenzhen 518055, P. R. China;* orcid.org/0000-0001-9361-2281; Email: li.jia@sz.tsinghua.edu.cn, thulijia@tsinghua.edu.cn

Authors

Hengyu Li − *Institute of Materials Research and Shenzhen Geim Graphene Center, Shenzhen International Graduate School, Tsinghua University, Shenzhen 518055, P. R. China*

Jie Wei − *Institute of Materials Research and Shenzhen Geim Graphene Center, Shenzhen International Graduate School, Tsinghua University, Shenzhen 518055, P. R. China*

Xuya Zhu − *Institute of Materials Research and Shenzhen Geim Graphene Center, Shenzhen International Graduate School, Tsinghua University, Shenzhen 518055, P. R. China*

Lin Gan − *Institute of Materials Research and Shenzhen Geim Graphene Center, Shenzhen International Graduate School, Tsinghua University, Shenzhen 518055, P. R. China;* orcid.org/0000-0003-3486-6016

Tao Cheng − *Institute of Functional Nano and Soft Materials (FUNSOM), Jiangsu Key Laboratory for Carbon-Based Functional Materials and Devices, Soochow University, Suzhou 215123, P. R. China;* orcid.org/0000-0003-4830-177X

Complete contact information is available at: https://pubs.acs.org/10.1021/acs.jpcc.2c01125

Notes

The authors declare no competing financial interest.

ACKNOWLEDGMENTS

This work was supported by the National Science Foundation of China (11874036, 52173222), the Guangdong Province Key Area R&D Program (2019B010940001, 2020B1212060015), the Local Innovative and Research Teams Project of Guangdong Pearl River Talents Program (2017BT01N111), and the Basic Research Project of Shenzhen, (JCYJ20200109142816479, WDZC20200819115243002). T.C. thanks the support from the Suzhou Key Laboratory of Functional Nano & Soft Materials, Collaborative Innovation Center of Suzhou Nano Science & Technology, the 111 Project, and the National Natural Science Foundation of China (21903058 and 22173066). Computational resources were provided by the Advanced Computing Center of Yunnan University and the Guangzhou Supercomputing Center.

REFERENCES

(1) Schwartz, S. E. Uncertainty in climate sensitivity: Causes, consequences, challenges. *Energy Environ. Sci.* **2008**, *1*, 430−453.

(2) Chu, S.; Majumdar, A. Opportunities and challenges for a sustainable energy future. *Nature* **2012**, *488*, 294−303.

(3) Zhang, B.; Zhang, J. Rational design of Cu-based electrocatalysts for electrochemical reduction of carbon dioxide. *J. Energy Chem.* **2017**, *26*, 1050−1066.

(4) Appel, A. M.; Bercaw, J. E.; Bocarsly, A. B.; Dobbek, H.; DuBois, D. L.; Dupuis, M.; Ferry, J. G.; Fujita, E.; Hille, R.; Kenis, P. J. A.; et al. Frontiers, opportunities, and challenges in biochemical and chemical catalysis of CO_2 fixation. *Chem. Rev.* **2013**, *113*, 6621−6658.

(5) Back, S.; Lim, J.; Kim, N.-Y.; Kim, Y.-H.; Jung, Y. Single-atom catalysts for CO_2 electroreduction with significant activity and selectivity improvements. *Chem. Sci.* **2017**, *8*, 1090−1096.

(6) Ju, W.; Bagger, A.; Hao, G.-P.; Varela, A. S.; Sinev, I.; Bon, V.; Roldan Cuenya, B.; Kaskel, S.; Rossmeisl, J.; Strasser, P. Understanding activity and selectivity of metal-nitrogen-doped carbon catalysts for electrochemical reduction of CO_2. *Nat. Commun.* **2017**, *8*, 944.

(7) Yang, H. B.; Hung, S.-F.; Liu, S.; Yuan, K.; Miao, S.; Zhang, L.; Huang, X.; Wang, H.-Y.; Cai, W.; Chen, R.; et al. Atomically dispersed Ni(I) as the active site for electrochemical CO_2 reduction. *Nat. Enery* **2018**, *3*, 140−147.

(8) Zhu, M.; Ye, R.; Jin, K.; Lazouski, N.; Manthiram, K. Elucidating the reactivity and mechanism of CO_2 electroreduction at highly dispersed cobalt phthalocyanine. *ACS Enery Lett.* **2018**, *3*, 1381−1386.

(9) Wu, H.; Zeng, M.; Zhu, X.; Tian, C.; Mei, B.; Song, Y.; Du, X.-L.; Jiang, Z.; He, L.; Xia, C.; et al. Defect engineering in polymeric

cobalt phthalocyanine networks for enhanced electrochemical CO_2 Reduction. *ChemElectroChem* **2018**, *5*, 2717−2721.
(10) Choi, J.; Wagner, P.; Gambhir, S.; Jalili, R.; MacFarlane, D. R.; Wallace, G. G.; Officer, D. L. Steric modification of a cobalt phthalocyanine/graphene catalyst to give enhanced and stable electrochemical CO_2 reduction to CO. *ACS Enery Lett.* **2019**, *4*, 666−672.
(11) Wang, M.; Torbensen, K.; Salvatore, D.; Ren, S.; Joulié, D.; Dumoulin, F.; Mendoza, D.; Lassalle-Kaiser, B.; Işci, U.; Berlinguette, C. P.; et al. CO_2 electrochemical catalytic reduction with a highly active cobalt phthalocyanine. *Nat. Commun.* **2019**, *10*, 3602.
(12) De Riccardis, A.; Lee, M.; Kazantsev, R. V.; Garza, A. J.; Zeng, G.; Larson, D. M.; Clark, E. L.; Lobaccaro, P.; Burroughs, P. W. W.; Bloise, E.; et al. Heterogenized pyridine-substituted cobalt(II) phthalocyanine yields reduction of CO_2 by tuning the electron affinity of the Co Center. *ACS Appl. Mater. Interfaces* **2020**, *12*, 5251−5258.
(13) Ren, S.; Joulié, D.; Salvatore, D.; Torbensen, K.; Wang, M.; Robert, M.; Berlinguette, C. P. Molecular electrocatalysts can mediate fast, selective CO_2 reduction in a flow cell. *Science* **2019**, *365*, 367−369.
(14) Zhang, Z.; Xiao, J.; Chen, X.-J.; Yu, S.; Yu, L.; Si, R.; Wang, Y.; Wang, S.; Meng, X.; Wang, Y.; et al. Reaction mechanisms of well-defined metal-N_4 sites in electrocatalytic CO_2 reduction. *Angew. Chem., Int. Ed.* **2018**, *57*, 16339−16342.
(15) Rollmann, L. D.; Iwamoto, R. T. Electrochemistry, electron paramagnetic resonance, and visible spectra of cobalt, nickel, copper, and metal-free phthalocyanines in dimethyl sulfoxide. *J. Am. Chem. Soc.* **1968**, *90*, 1455−1463.
(16) Mahmood, M. N.; Masheder, D.; Harty, C. J. Use of gas-diffusion electrodes for high-rate electrochemical reduction of carbon dioxide. II. Reduction at metal phthalocyanine-impregnated electrodes. *J. Appl. Electrochem.* **1987**, *17*, 1223−1227.
(17) Abe, T.; Taguchi, F.; Yoshida, T.; Tokita, S.; Schnurpfeil, G.; Wöhrle, D.; Kaneko, M. Electrocatalytic CO_2 reduction by cobalt octabutoxyphthalocyanine coated on graphite electrode. *J. Mol. Catal. A: Chem.* **1996**, *112*, 55−61.
(18) Xia, Y.; Kashtanov, S.; Yu, P.; Chang, L.-Y.; Feng, K.; Zhong, J.; Guo, J.; Sun, X. Identification of dual-active sites in cobalt phthalocyanine for electrochemical carbon dioxide reduction. *Nano Energy* **2020**, *67*, 104163.
(19) Liu, Y.; Deb, A.; Leung, K. Y.; Nie, W.; Dean, W. S.; Penner-Hahn, J. E.; McCrory, C. C. L. Determining the coordination environment and electronic structure of polymer-encapsulated cobalt phthalocyanine under electrocatalytic CO_2 reduction conditions using in situ X-Ray absorption spectroscopy. *Dalton Trans.* **2020**, *49*, 16329−16339.
(20) Corbin, N.; Zeng, J.; Williams, K.; Manthiram, K. Heterogeneous molecular catalysts for electrocatalytic CO_2 reduction. *Nano Res.* **2019**, *12*, 2093−2125.
(21) Zeng, J. S.; Corbin, N.; Williams, K.; Manthiram, K. Kinetic analysis on the role of bicarbonate in carbon dioxide electroreduction at immobilized cobalt phthalocyanine. *ACS Catal.* **2020**, *10*, 4326−4336.
(22) Abe, T.; Imaya, H.; Yoshida, T.; Tokita, S.; Schlettwein, D.; Wöhrle, D.; Kaneko, M. Electrochemical CO_2 reduction catalysed by cobalt octacyanophthalocyanine and its mechanism. *J. Porphyrins Phthalocyanines* **1997**, *1*, 315−321.
(23) Zhang, X.; Wu, Z.; Zhang, X.; Li, L.; Li, Y.; Xu, H.; Li, X.; Yu, X.; Zhang, Z.; Liang, Y.; et al. Highly selective and active CO_2 reduction electrocatalysts based on cobalt phthalocyanine/carbon nanotube hybrid structures. *Nat. Commun.* **2017**, *8*, 14675.
(24) Morlanés, N.; Takanabe, K.; Rodionov, V. Simultaneous reduction of CO_2 and splitting of H_2O by a single immobilized cobalt phthalocyanine electrocatalyst. *ACS Catal.* **2016**, *6*, 3092−3095.
(25) Wang, X.; Cai, Z. F.; Wang, Y. Q.; Feng, Y. C.; Yan, H. J.; Wang, D.; Wan, L. J. In-situ scanning tunneling microscopy of cobalt-phthalocyanine-catalyzed CO_2 reduction reaction. *Angew. Chem., Int. Ed.* **2020**, *59*, 16098−16103.
(26) Kresse, G.; Furthmüller, J. Efficiency of ab-initio total energy calculations for metals and semiconductors using a plane-wave basis set. *Comput. Mater. Sci.* **1996**, *6*, 15−50.
(27) Kresse, G.; Furthmüller, J. Efficient iterative schemes for ab initio total-energy calculations using a plane-wave basis set. *Phys. Rev. B* **1996**, *54*, 11169−11186.
(28) Krukau, A. V.; Vydrov, O. A.; Izmaylov, A. F.; Scuseria, G. E. Influence of the exchange screening parameter on the performance of screened hybrid functionals. *J. Chem. Phys.* **2006**, *125*, 224106.
(29) Anisimov, V. I.; Zaanen, J.; Andersen, O. K. Band theory and Mott insulators: Hubbard U instead of Stoner I. *Phys. Rev. B* **1991**, *44*, 943−954.
(30) Liechtenstein, A. I.; Anisimov, V. I.; Zaanen, J. Density-functional theory and strong interactions: Orbital ordering in Mott-Hubbard insulators. *Phys. Rev. B* **1995**, *52*, R5467−R5470.
(31) Brumboiu, I. E.; Haldar, S.; Lüder, J.; Eriksson, O.; Herper, H. C.; Brena, B.; Sanyal, B. Influence of electron correlation on the electronic structure and magnetism of transition-metal phthalocyanines. *J. Chem. Theory Comput.* **2016**, *12*, 1772−1785.
(32) Grimme, S. Semiempirical GGA-type density functional constructed with a long-range dispersion correction. *J. Comput. Chem.* **2006**, *27*, 1787−1799.
(33) Grimme, S.; Antony, J.; Ehrlich, S.; Krieg, H. A consistent and accurate ab initio parametrization of density functional dispersion correction (DFT-D) for the 94 elements H-Pu. *J. Chem. Phys.* **2010**, *132*, 154104.
(34) Mathew, K.; Sundararaman, R.; Letchworth-Weaver, K.; Arias, T. A.; Hennig, R. G. Implicit solvation model for density-functional study of nanocrystal surfaces and reaction pathways. *J. Chem. Phys.* **2014**, *140*, 084106.
(35) Fishman, M.; Zhuang, H. L.; Mathew, K.; Dirschka, W.; Hennig, R. G. Accuracy of exchange-correlation functionals and effect of solvation on the surface energy of copper. *Phys. Rev. B* **2013**, *87*, 245402.
(36) Pliego, J. R.; Riveros, J. M. Theoretical calculation of pKa using the cluster-continuum model. *J. Phys. Chem. A* **2002**, *106*, 7434−7439.
(37) Göttle, A. J.; Koper, M. T. M. Proton-coupled electron transfer in the electrocatalysis of CO_2 reduction: prediction of sequential vs. concerted pathways using DFT. *Chem. Sci.* **2017**, *8*, 458−465.
(38) Mathew, K.; Kolluru, V. S. C.; Mula, S.; Steinmann, S. N.; Hennig, R. G. Implicit self-consistent electrolyte model in plane-wave density-functional theory. *J. Chem. Phys.* **2019**, *151*, 234101.
(39) Roy, L. E.; Jakubikova, E.; Guthrie, M. G.; Batista, E. R. Calculation of one-electron redox potentials revisited. Is it possible to calculate accurate potentials with density functional methods? *J. Phys. Chem. A* **2009**, *113*, 6745−6750.
(40) Galstyan, A.; Knapp, E.-W. Accurate redox potentials of mononuclear iron, manganese, and nickel model complexes. *J. Comput. Chem.* **2009**, *30*, 203−211.
(41) Granda-Marulanda, L. P.; Rendón-Calle, A.; Builes, S.; Illas, F.; Koper, M. T. M.; Calle-Vallejo, F. A semiempirical method to detect and correct DFT-based gas-phase errors and its application in electrocatalysis. *ACS Catal.* **2020**, *10*, 6900−6907.
(42) Nørskov, J. K.; Rossmeisl, J.; Logadottir, A.; Lindqvist, L.; Kitchin, J. R.; Bligaard, T.; Jónsson, H. Origin of the overpotential for oxygen reduction at a fuel-cell cathode. *J. Phys. Chem. B* **2004**, *108*, 17886−17892.
(43) Henkelman, G.; Uberuaga, B. P.; Jónsson, H. A climbing image nudged elastic band method for finding saddle points and minimum energy paths. *J. Chem. Phys.* **2000**, *113*, 9901−9904.
(44) Henkelman, G.; Jónsson, H. Improved tangent estimate in the nudged elastic band method for finding minimum energy paths and saddle points. *J. Chem. Phys.* **2000**, *113*, 9978−9985.
(45) Lu, X.; Ahsaine, H. A.; Dereli, B.; Garcia-Esparza, A. T.; Reinhard, M.; Shinagawa, T.; Li, D.; Adil, K.; Tchalala, M. R.; Kroll, T.; et al. Operando elucidation on the working state of immobilized fluorinated iron porphyrin for selective aqueous electroreduction of CO_2 to CO. *ACS Catal.* **2021**, *11*, 6499−6509.

https://doi.org/10.1021/acs.jpcc.2c01125
J. Phys. Chem. C 2022, 126, 9665−9672

(46) Huang, Y.; Nielsen, R. J.; Goddard, W. A. Reaction mechanism for the hydrogen evolution reaction on the basal plane sulfur vacancy site of MoS_2 using grand canonical potential kinetics. *J. Am. Chem. Soc.* **2018**, *140*, 16773−16782.
(47) Mason, R.; Williams, G. A.; Fielding, P. E. Structural chemistry of phthalocyaninato-cobalt(II) and -manganese(II). *J. Chem. Soc., Dalton Trans.* **1979**, 676−683.
(48) Ellis, T. S.; Park, K. T.; Ulrich, M. D.; Hulbert, S. L.; Rowe, J. E. Interaction of metallophthalocyanines (MPc, M=Co, Ni) on Au(001): Ultraviolet photoemission spectroscopy and low energy electron diffraction study. *J. Appl. Phys.* **2006**, *100*, 093515.
(49) Grobosch, M.; Schmidt, C.; Kraus, R.; Knupfer, M. Electronic properties of transition metal phthalocyanines: The impact of the central metal atom (d5-d10). *Org. Electron.* **2010**, *11*, 1483−1488.
(50) Ouyang, J.; Shigehara, K.; Yamada, A.; Anson, F. C. Hexadecafluoro- and octacyano phthalocyanines as electrocatalysts for the reduction of dioxygen. *J. Electroanal. Chem. Interfacial Electrochem.* **1991**, *297*, 489−498.
(51) Lieber, C. M.; Lewis, N. S. Catalytic reduction of carbon dioxide at carbon electrodes modified with cobalt phthalocyanine. *J. Am. Chem. Soc.* **1984**, *106*, 5033−5034.
(52) Leung, K.; Nielsen, I. M. B.; Sai, N.; Medforth, C.; Shelnutt, J. A. Cobalt−porphyrin catalyzed electrochemical reduction of carbon dioxide in water. 2. Mechanism from first principles. *J. Phys. Chem. A* **2010**, *114*, 10174−10184.
(53) Han, N.; Wang, Y.; Ma, L.; Wen, J.; Li, J.; Zheng, H.; Nie, K.; Wang, X.; Zhao, F.; Li, Y.; et al. Supported cobalt polyphthalocyanine for high-performance electrocatalytic CO_2 reduction. *Chem* **2017**, *3*, 652−664.
(54) Chen, J.; Zhu, M.; Li, J.; Xu, J.; Han, Y.-F. Structure-activity relationship of the polymerized cobalt phthalocyanines for electrocatalytic carbon dioxide reduction. *J. Phys. Chem. C* **2020**, *124*, 16501−16507.
(55) Chen, X.; Wei, D.; Ahlquist, M. S. G. Aggregation and significant difference in reactivity therein: blocking the CO_2-to-CH_3OH reaction. *Organometallics* **2021**, *40*, 3087−3093.
(56) Vijay, S.; Gauthier, J. A.; Heenen, H. H.; Bukas, V. J.; Kristoffersen, H. H.; Chan, K. Dipole-field interactions determine the CO2 reduction activity of 2D Fe-N-C single-atom catalysts. *ACS Catal.* **2020**, *10*, 7826−7835.
(57) Hansch, C.; Leo, A.; Taft, R. W. A survey of Hammett substituent constants and resonance and field parameters. *Chem. Rev.* **1991**, *91*, 165−195.

https://doi.org/10.1021/acs.jpcc.2c01125
J. Phys. Chem. C 2022, 126, 9665−9672